analytical chemistry

Article

Cite This: *Anal. Chem.* XXXX, XXX, XXX−XXX

pubs.acs.org/ac

Glycopeptide Nanofiber Platform for Aβ-Sialic Acid Interaction Analysis and Highly Sensitive Detection of Aβ

Li Lei, Rui Geng, Zhiai Xu,* Yijing Dang, Xianli Hu, Lingling Li, Ping Geng, Yang Tian, and Wen Zhang*

School of Chemistry and Molecular Engineering, East China Normal University, Shanghai 200241, China

Supporting Information

ABSTRACT: The variation of amyloid β peptide (Aβ) concentration and Aβ aggregation are closely associated with the etiology of Alzheimer's diseases (AD). The interaction of Aβ with the monosialoganglioside-rich neuronal cell membrane has been suggested to influence Aβ aggregation. Therefore, studies on the mechanism of Aβ and sialic acids (SA) interaction would greatly contribute to better understanding the pathogenesis of AD. Herein, we report a novel approach for Aβ−SA interaction analysis and highly sensitive Aβ detection by mimicing the cell surface presentation of SA clusters through engineering of SA-modified peptide nanofiber (SANF). The SANF displayed well-ordered 1D nanostructure with high density of SA on surface. Using FAM-labeled Aβ fragments of $Aβ_{1-16}$, $Aβ_{16-23}$, and $Aβ_{24-40}$, the interaction between Aβ and SA was evaluated by the fluorescence titration experiments. It was found that the order of the SA-binding affinity was $Aβ_{1-16}$ > $Aβ_{24-40}$ > $Aβ_{16-23}$. Importantly, the presence of full-length $Aβ_{1-40}$ monomer triggered a significant fluorescence enhancement due to the multivalent binding of $Aβ_{1-40}$ to the nanofiber. This fluorescent turn-on response showed high selectivity and sensitivity for $Aβ_{1-40}$ detection and the method was further used for Aβ aggregation process monitoring and inhibitor screening. The results suggest the proposed strategy is promising to serve as a tool for mechanism study and the early diagnosis of Alzheimer's disease.

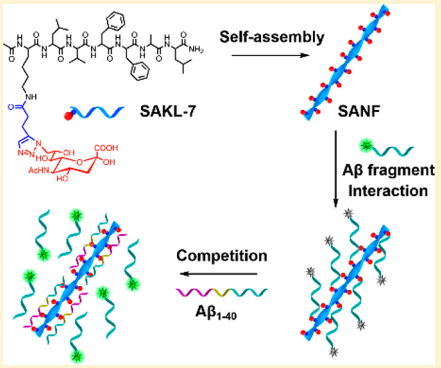

Alzheimer's disease (AD) is a chronic neurodegenerative disease which brings huge burden to the patients and their family. Up to now, there are no effective strategies to cure AD, but an early diagnosis and treatment would be beneficial to ameliorate the symptoms of this terrible disease. Amyloid β peptide (Aβ) is the major component of senile plaques in AD and it is believed to be linked with the pathogenesis of AD.[1−5] Aβ is produced from the proteolytic process of amyloid precursor protein (APP) by β- and γ-secretases.[6,7] Under aberrant conditions, extracellular Aβ would aggregate into oligomers, protofibrils and fibrils, and Aβ accumulation in the brain are thought to be associated with the neurotoxicity.[8−12] Aβ aggregation disrupts the homeostasis and results in the variation of Aβ content in the cerebrospinal fluid (CSF). Importantly, the changes of the Aβ level occur in the early stage of AD development.[13−15] Therefore, monitoring Aβ concentration alteration is critical and could provide a promising way for preclinical AD diagnosis.

Aβ aggregation could impair neurons by interaction with cell membranes. Since monosialoganglioside GM1-bound Aβ was discovered in brains of AD patients,[16,17] it has also been suggested that Aβ interaction with neuronal lipid membranes would greatly influence the aggregation behavior and contribute to the neurotoxicity.[18−22] GM1 gangliosides are sialic acid (SA)-containing glycosphingolipids which are abundant in neuronal membranes in the form of clusters.[16,23−25] A series of in vitro investigations have demonstrated that GM1 has a significant effect on the conformation of Aβ peptides, then it would accelerate or inhibit oligomerization and fibrillation in the following processes depending on the ganglioside concentration.[25−30] To exactly decipher the role of GM1 in Aβ aggregation, fully understanding the Aβ-GM1 interaction at the molecular level is essential. Recently, molecular dynamics (MD) simulations were performed to analyze the physicochemical interaction of $Aβ_{1-40}$ with GM1 and it showed that $Aβ_{1-40}$ inserted into the lipid membrane through hydrogen bonds between His 13 or His 14 and Leu 34 of Aβ and the membrane.[31,32] Nevertheless, versatile and sensitive methods to explore the interaction of Aβ with the SA epitopes experimentally are limited and highly desired.

SA epitopes are present as clusters on membrane, which display multivalent interaction with proteins or other receptors.[33,34] To better understand the nature of interactions, mimicking the cell surface that display multivalent ligands is a rational option.[35,36] Many researchers have attempted to synthesize biomimetic nanostructures using polymers, inorganic nanomaterials and peptides that display multiple ligands for the applications such as enhanced targeting, protein activation and inhibition of biological pathogens.[37−40] Among these materials, the self-assembled peptide nanostructures hold

Received: January 22, 2019
Accepted: June 4, 2019

DOI: 10.1021/acs.analchem.9b00377
Anal. Chem. XXXX, XXX, XXX−XXX

unique features including well-defined morphologies, tailorable functionality, and good biocompatibility.[41−43]

Herein, we have prepared the glycopeptide nanofiber for Aβ−SA interaction analysis based on the self-assembly of SA-modified peptide and developed it for highly sensitive Aβ detection. SA moieties were covalently conjugated onto the Ac-KLVFFAL-NH_2 (KL-7) peptide using one alkyne linker by click chemistry (named as SAKL-7, Scheme 1). The self-assembly of SAKL-7 resulted in the formation of nanofiber (SANF), which was characterized by a high density of SA decorated on the surface. The SANF were then evaluated for their ability to recognize different FAM-labeled Aβ fragments of $A\beta_{1-16}$, $A\beta_{16-23}$, and $A\beta_{24-40}$. The experimental studies based on the fluorescence quenching effect clarified that Aβ could bind tightly to the SANF surface. The binding affinity of SA and Aβ followed the order of $A\beta_{1-16}$ > $A\beta_{24-40}$ > $A\beta_{16-23}$. The full-length $A\beta_{1-40}$ monomer induced the fluorescence recovery of the SANF−$A\beta_{24-40}$ system owing to the specific multivalent interaction between $A\beta_{1-40}$ and SA. A fluorescent turn-on strategy with high sensitivity and selectivity for detecting Aβ and Aβ aggregation study was successfully proposed.

Scheme 1. Preparation of PAKL-7 and SAKL-7 and Their Self-Assembly into Nanofibers

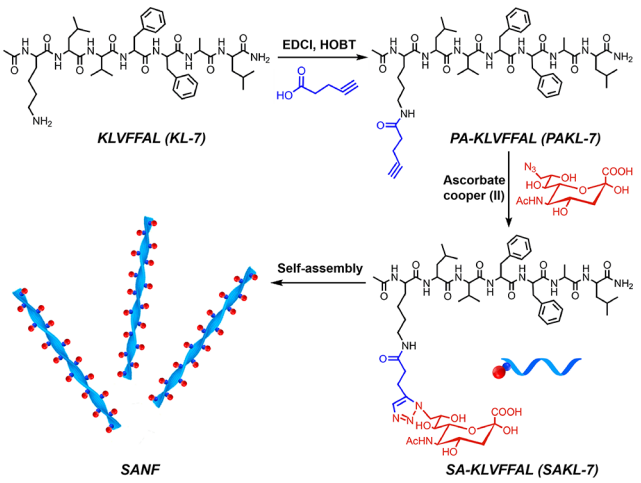

EXPERIMENTAL SECTION

Chemicals and Reagents. The peptide Ac-KLVFFAL-NH_2 (KL-7) and the FAM-labeled Aβ fragments were purchased from GL Biochem, Ltd. (Shanghai, China). $A\beta_{1-40}$ (DAEFR HDSGY EVHHQ KLVFF AEDVG SNKGA IIGLM VGGVV) was obtained from American Peptide Co. (CA, USA). 1,1,1,3,3,3-Hexafluoro-2-propanol (HFIP), trifluoroacetic acid (TFA), and *p*-toluenesulfonyl chloride (*p*-TsCl) were bought from Tokyo Chemical Industry (TCI) Co., Ltd. (Shanghai, China). Thioflavin T (ThT), (−)-epigallocatechin gallate (EGCG), glutathione (GSH), bovine serum albumin (BSA), *N*-acetylneuraminic acid (Neu5Ac), pyridine, resorcinol, and 4-pentynoic acid (PA) were purchased from Sigma-Aldrich Ltd. (Shanghai, China). Dialysis bags with a molecular weight cut off (MWCO) of 500 Da were obtained from Yuanye Biotechnology Co., Ltd. (Shanghai, China). All other chemicals are of analytical grade except those noted otherwise and used directly without further purification. Water (18.2 MΩ·cm) from a laboratory water purification system (Hitech Instruments Co., Ltd.) was used throughout the experiment.

Measurements. Transmission electron microscopy (TEM) measurements were collected with a HT7700 transmission electron microscope (Hitachi, Tokyo, Japan). Atomic force microscopy (AFM) images were obtained on a Dimension FastScan (Bruker, Germany) using tapping mode under ambient condition. Infrared spectra were performed on a Nicolet 500 Fourier Transform Infrared (FT-IR) spectrometer (Madison, WI). Circular dichroism (CD) spectra were obtained using a Chirascan spectropolarimeter (Applied Photophysics, UK). Proton nuclear magnetic resonance (^{1}H NMR) and carbon nuclear magnetic resonance spectra (^{13}C NMR) were measured by using a Bruker 500 MHz NMR spectrometer at 25 °C. The ultraviolet−visible (UV−vis) absorption and fluorescence spectra were obtained by a Cary 60 UV−vis spectrophotometer and a Cary Eclipse spectrofluorophotometer, respectively (Agilent Technologies, Palo Alto, CA, USA). The zeta potential measurement was conducted at 25 °C using a Malvern Zetasizer Nanoseries (Malvern, England). The mass spectra were measured with a LC-MS spectrometer (Bruker, Germany).

Synthesis of SA-ME. A 500.0 mg amount of Neu5Ac (1.6 mmol) and 30 μL of TFA were added to 10 mL of anhydrous MeOH in the flasks. Then the solution reacted at room temperature with stirring until it was clarified. The solvent was removed by evaporation, and SA-ME was obtained as a white solid (484.5 mg, 1.5 mmol) in 93.8% yield. The solid product was dried over P_2O_5 in vacuo overnight for further use. ^{1}H NMR (500 MHz, CD_3OD) δ 4.07−3.98 (m, 2H), 3.82 (dd, *J* = 13.3, 6.6 Hz, 2H), 3.80 (m, 3H), 3.72 (ddd, *J* = 8.8, 5.7, 2.9 Hz, 1H), 3.64 (dd, *J* = 11.3, 5.7 Hz, 1H), 3.50 (dd, *J* = 9.2, 1.4 Hz, 1H), 3.33 (s, 3H), 2.24 (m, 1H), 2.03 (s, 3H), 1.91 (t, iJ = 12.9, 11.4 Hz, 1H). ^{13}C NMR (100 MHz, CD_3OD) δ 175.11 (s), 171.77 (s), 96.66 (s), 72.07 (s), 71.64 (s), 70.18 (s), 67.85 (s), 64.83 (s), 54.31 (s), 53.14 (s), 40.69 (s), 22.65 (s). MS calcd for $C_{12}H_{21}O_9N$, 323.20; found, 346.11 (M + Na^+).

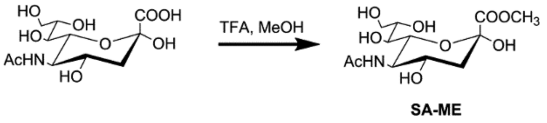

Synthesis of Ts-SA. A 500.0 mg amount of solid SA-ME (1.5 mmol) was coevaporated with dry pyridine twice to remove a trace amount of water and then dissolved in 6 mL of pyridine. The solution was cooled to 0 °C, and *p*-TsCl (600.0 mg, 3.2 mmol) was added. The mixture was allowed to stay at room temperature and stirred overnight. After removing pyridine, the residue was purified by column chromatography (EtOAc:MeOH = 15:1) to gain Ts-SA as a white solid (572.0 mg, 1.2 mmol) in 80.0% yield. ^{1}H NMR (500 MHz, CD_3OD) δ 7.81 (d, *J* = 8.3 Hz, 2H), 7.46 (d, *J* = 8.1 Hz, 2H), 4.29 (dd, *J* = 10.0, 2.2 Hz, 1H), 4.10−4.02 (m, 2H), 3.97 (d, *J* = 10.5 Hz, 1H), 3.90−3.86 (m, 1H), 3.81 (d, *J* = 4.6 Hz, 1H), 3.79−3.74 (m, 4H), 3.45 (t, *J* = 9.7 Hz, 1H), 3.34 (dd, *J* = 11.2, 9.7 Hz, 3H), 2.47 (s, 3H), 2.23 (dd, *J* = 12.9, 4.9 Hz, 1H), 2.04 (s, 3H), 1.80 (m, 1H). ^{13}C NMR (100 MHz, CD_3OD) δ 175.16 (s), 171.88 (s), 146.42 (s), 134.15 (s), 131.02 (s), 129.05 (s), 129.02 (d, *J* = 9.2 Hz), 126.95 (s), 96.61 (s), 73.63 (s), 71.70 (s), 69.93 (s), 69.28 (s), 67.64 (s), 54.09 (s), 53.29 (s), 40.71 (s), 22.67 (d, J = 19.4 Hz), 21.62 (d, J = 13.7 Hz). MS calcd for $C_{19}H_{27}O_{11}NS$; 477.12, found, 500.12 (M + Na^+).

DOI: 10.1021/acs.analchem.9b00377
Anal. Chem. XXXX, XXX, XXX−XXX

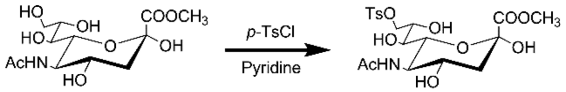

Ts-SA

Synthesis of N_3−SA. An 800 mg mount of sodium azide (12.0 mmol), 1400 mg of Ts-SA (3.0 mmol), and deionized water (5 mL) were added to acetone (15 mL). The mixture was heated under reflux overnight. Then the solvent was completely removed, and the residues were purified by column chromatography to afford N_3−SA as a pale yellow solid (798 mg, 2.4 mmol, 80.1%). ^{1}H NMR (500 MHz, D_2O) δ 3.93 (d, J = 6.5 Hz, 1H), 3.89 (d, J = 12.8 Hz, 1H), 3.85 (ddd, J = 14.6, 10.1, 8.2 Hz, 1H), 3.82 (d, J = 3.5 Hz, 1H), 3.54 (d, J = 2.7 Hz, 1H), 3.51−3.43 (m, 2H), 3.41−3.36 (m, 1H), 3.27 (s, 1H), 2.19−2.04 (m, 2H), 1.99 (s, 3H), 1.81 (d, J = 20.0 Hz, 1H), 1.73 (d, J = 11.7 Hz, 1H). ^{13}C NMR (100 MHz, D_2O) δ 176.24 (s), 174.29 (s), 96.01 (s), 69.61 (s), 68.67 (s), 68.43 (s), 66.78 (s), 53.38 (s), 51.80 (s), 38.92 (s), 21.64 (s). MS calcd for $C_{11}H_{18}N_4O_8$, 334.10; found, 357.10 (M + Na^+).

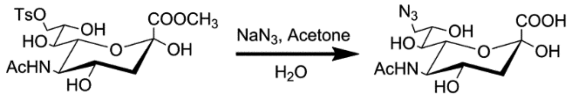

N_3-SA

Synthesis of PAKL-7. Briefly, PA were dissolved in DMSO and then activated with EDCI, HOBT, and DMAP (PA:EDCI:HOBT:DMAP = 1:3:3:3) for 2 h at room temperature under N_2 atmosphere. Then the peptide KL-7 (dissolved in DMSO) solution was dropwise added to the PA solutions with gentle agitation, and the mixture was reacted for 24 h at room temperature. Then it was purified with dialysis bags (MWCO, 500) to remove unreacted PA and other ions. Later, a white solid was obtained under reduced pressure and stored at 4 °C for further use. MS calcd for $C_{51}H_{75}N_9O_9$, 957.65; found, 980.56 (M + Na^+).

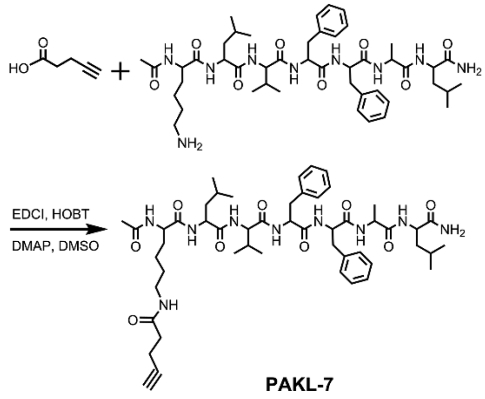

PAKL-7

Synthesis of SAKL-7. A 140 mg amount of N_3−SA (0.150 mmol) and 89.1 mg of sodium ascorbate (0.450 mmol) were added to a stirred solution of 100 mg of PAKL-7 (0.104 mmol) in DMF (6.00 mL), followed by the addition of 1.00 M $CuSO_4$ (45.0 μL). The reaction mixture was stirred at room temperature for 24 h, and then it was purified with dialysis bags (MWCO, 500). Later, a white solid was obtained under reduced pressure and stored at 4 °C for further use. MALDI-TOF MS calcd for $C_{62}H_{93}N_{13}O_{17}$, 1291.68; found, 1290.67 (M − H).

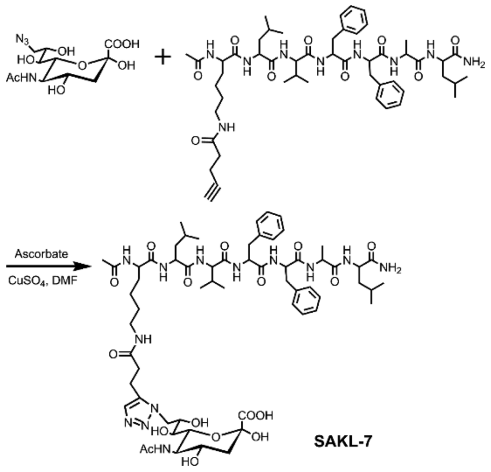

SAKL-7

Peptide Self-Assembly. Briefly, 3.5 mM SAKL-7 and PAKL-7 peptide were dissolved in a 2:1 (v/v) mixture of DMSO/water, respectively. Then they were allowed to assemble for approximately 24 h in a 37 °C water bath and ready for use.

Quantitative Estimation of SA on Nanofiber Surface. SA amount modified on the nanofiber surface was determined according to the literature.[44] Briefly, 20 μL of Neu5Ac (5−40 μg/mL) or 20 μL of SANF (1 mg/mL) was added to the solution containing 0.1 M $CuSO_4$, 4% resorcinol reagent, and hydrochloric acid. Then the mixture was heated for 15 min in a boiling water bath. After heating, the solutions were immediately cooled in running water, and the absorbance was detected by a UV−vis spectrophotometer.

Preparation of Aβ_{1-40} Samples. Lyophilized Aβ_{1-40} peptides powder was dissolved in HFIP, and then HFIP solution containing Aβ_{1-40} (1 mg/mL) was put in the ice−water bath for 20 min for further dissolution. HFIP was evaporated by treatment of N_2 flow to get a thin film and stored at −20 °C before use. The Aβ_{1-40} monomer solution (10 μM) was prepared by dissolving the Aβ_{1-40} film in 10 mM Tris-HCl buffer (pH 7.4) in the dark and used at once. The Aβ_{1-40} oligomer and fibril were obtained by incubating Aβ_{1-40} solution at 37 °C for 6 and 48 h, respectively. The Aβ_{1-40} aggregation study was performed as follows: Aβ_{1-40} solution was mixed with 10 mM GSH or EGCG, and then the mixture was incubated at 37 °C for different times.

SA and Aβ Interaction Analysis. For the assay, the mixture comprising a fixed concentration (7 μM) of FAMDK$_{16}$ (FAM-DAEFRHDSGYEVHHQK), FAMKD$_8$ (FAM-KLVFFAED), or FAMVV$_{17}$ (FAM-VGSNKGAIIGLMVGGVV) and varying concentrations of SANF in 10 mM Tris-HCl buffer (pH 7.4) was prepared. The mixing solutions were allowed to react further for 30 min at room temperature in the dark. The fluorescence was then detected by a fluorescence spectrophotometer. For the contrast assay, the SANF was replaced by PANF.

Fluorescence Turn-on Assay. The fluorescence turn-on assay was fabricated by incubating 350 μM SANF and 7 μM FAMVV$_{17}$ aqueous solution at room temperature for 30 min. Then Aβ_{1-40} of different concentrations in the 10 mM Tris-HCl buffer (pH 7.4) were added into the above mixture. The change of FAM fluorescence was detected by a fluorescence spectrophotometer by excitation with 462 nm light. For comparison, BSA samples of different concentrations were also examined.

DOI: 10.1021/acs.analchem.9b00377
Anal. Chem. XXXX, XXX, XXX−XXX

Determination of $A\beta_{1-40}$ in Artificial Cerebrospinal Fluid and Fetal Bovine Serum. The artificial cerebrospinal fluid (aCSF) was prepared by mixing NaCl (126 mM), KCl (2.4 mM), KH_2PO_4 (0.5 mM), $MgCl_2$ (0.85 mM), $CaCl_2$ (1.1 mM), $NaHCO_3$ (27.5 mM), and Na_2SO_4 (0.5 mM) into doubly distilled water, and the solution pH was adjusted to 7.4. The calibration curve was first established by detecting the fluorescence intensity of FAM in the mixture containing 7 μM $FAMVV_{17}$ and 350 μM SANF solutions upon addition of $A\beta_{1-40}$ at a series of concentrations. Then the aCSF samples containing three $A\beta_{1-40}$ concentrations were detected.

To test the applicability of $A\beta_{1-40}$ detection in serum, a series of fetal bovine serum (FBS) samples containing $A\beta_{1-40}$ in FBS were prepared by spiking $A\beta_{1-40}$ into FBS. Then 20 μL of FBS with different concentrations of $A\beta_{1-40}$ were added to 180 μL of mixed solution, which consisted of 350 μM SANF and 7 μM $FAMVV_{17}$. After incubating for 30 min, the change of FAM fluorescence was detected. The results were validated by using human $A\beta_{1-40}$ ELISA kits (Elabscience Biotechnology, China) following the manufacturer's instructions.

$A\beta_{1-40}$ Aggregation Assay. To test the applicability of the method for $A\beta_{1-40}$ aggregation assay, 350 μM SANF and 7 μM $FAMVV_{17}$ were mixed with (i) 10 μM $A\beta_{1-40}$, (ii) 10 μM $A\beta_{1-40}$ with EGCG, or (iii) 10 μM $A\beta_{1-40}$ with GSH incubated in 10 mM Tris-HCl buffer (pH 7.4) for a certain time. The fluorescence spectra were monitored by a fluorescence spectrophotometer.

RESULTS AND DISCUSSION

Design and Synthesis of Glycosylated Peptide. The peptide sequence containing the FF nucleating core is known to have a high propensity to self-assemble into diverse nanostructures through electrostatic, $\pi-\pi$ stacking, and hydrophobic interactions.[45−48] Recently, much attention has been focused on their use in material fields and biotechnology because of their high stability and biocompatibility.[48−50] To obtain glycan clusters in a highly ordered array based on the supramolecular self-assembly, the KL-7 peptide containing FF with the ability to form β-sheets and a terminal K residue for further glycosylation is selected. Subsequently, 4-pentynoic acid (PA) was introduced by covalent coupling with lysine to serve as the conjugation site for saccharide (PAKL-7). Neu5Ac (a representative of SA) was then covalently linked to the peptide PAKL-7 by click chemistry, forming an amphiphilic glycosylated peptide (SAKL-7) (Scheme 1).

To verify the successful coupling of PA on KL-7 peptide, the chemical structure of the resultant PAKL-7 was characterized by nuclear magnetic resonance (NMR), Fourier transform infrared (FT-IR) spectra, and high-resolution mass spectra (HRMS). New characteristic peaks of CH_2 assigned to PA appeared at 2.4−2.2 ppm in the ^{1}H NMR spectrum of PAKL-7 (Figures S1 and S2), suggesting the successful covalent attachment of PA. Moreover, the FT-IR spectra showed the characteristic absorption bond at 2127 cm^{-1} assigned to C≡C stretching in the PAKL-7 (Figure S3). Meanwhile, the molecular ion peak at 980.56 ($M + Na^+$) in HRMS spectra revealed the successful synthesis of PAKL-7 (Figures S4 and S5).

Next, SA was conjugated on PAKL-7 via copper(I)-catalyzed alkyne−azide cycloaddition (CuAAC) with N_3−SA to obtain SAKL-7. N_3−SA was synthesized and characterized by carbon nuclear magnetic resonance spectroscopy (^{13}C NMR), ^{1}H NMR, FT-IR spectra, and HRMS (Figures S6−15). As can be seen from Figure S16, the ^{1}H NMR spectrum at 3.9−3.5 ppm of SAKL-7 revealed the presence of SA by comparing that of free N_3−SA (Figure S10) and PAKL-7 (Figure S1). Furthermore, the absence of a peak at 2127 cm^{-1} of the C≡C stretching of PAKL-7 in the FT-IR spectra of SAKL-7 (Figure S17) as well as HRMS at 1290.67 (M − H) (Figure S18) confirmed the successful preparation of SAKL-7.

Glycopeptide Self-Assembly. We first studied the capacity of SAKL-7 and PAKL-7 to self-assemble into supramolecular nanostructures by transmission electron microscopy (TEM). As shown in Figure 1A and 1B, TEM

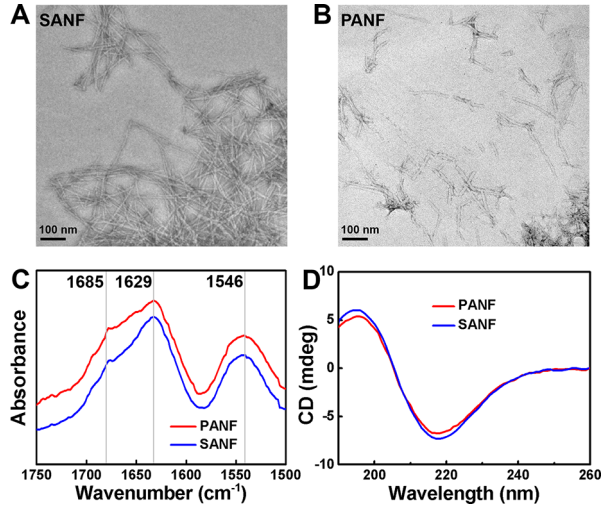

Figure 1. TEM images of SANF (A) and PANF (B). (C) FT-IR spectra of PANF and SANF. (D) CD spectra of PANF and SANF.

images after negative staining obviously show that the SANF and PANF have similar fibril morphology. SAKL-7 and PAKL-7 formed high-aspect-ratio filaments with a diameter of approximately 12 nm and length up to 300 nm in the mixed solvent of DMSO and water. Zeta potential measurements were carried out to characterize the surface charge of these assembled nanostructures. The conversion of positively charged PANF (4.8 ± 0.5 mV) to negatively charged SANF (−19.6 ± 1.2 mV) as shown in Figure S19 suggested the covalent grafting of SA onto the surface of peptide nanofiber. The SA grafting ratio was determined according to a previous method, and it showed that 73.6% of the KL-7 peptides were modified with SA (Figure S20),[44] indicating that plenty of sialic acids were exposed on the surface of nanofiber. FT-IR and circular dichroism (CD) spectroscopy were utilized to characterize the secondary structure of the peptide nanofiber. Both SANF and PANF showed a strong amide I absorption band at 1629 cm^{-1}, which indicated H-bonded β-sheet structures. Weak absorption bands observed at 1685 cm^{-1} could be attributed to the antiparallel configuration (Figure 1C).[51,52] Amide II bands at 1546 cm^{-1} were observed for SANF and PANF. Both of the self-assembled supramolecular structures exhibited negative peaks near 218 nm in the CD spectra (Figure 1D), indicating the presence of β-sheet conformation.[52,53]

Interaction of SA with Different $A\beta$ Fragments. To clearly investigate the interaction profile of $A\beta_{1-40}$ with SA, the $A\beta_{1-40}$ peptides were separated into three parts: the N-terminal residues of $A\beta_{1-16}$, the core residues of $A\beta_{16-23}$, and the C-terminal residues of $A\beta_{24-40}$, each of which was labeled

DOI: 10.1021/acs.analchem.9b00377
Anal. Chem. XXXX, XXX, XXX−XXX

with fluorophore FAM and designated as FAMDK$_{16}$, FAMKD$_8$, and FAMVV$_{17}$, respectively (Figure 2A). Fluo-

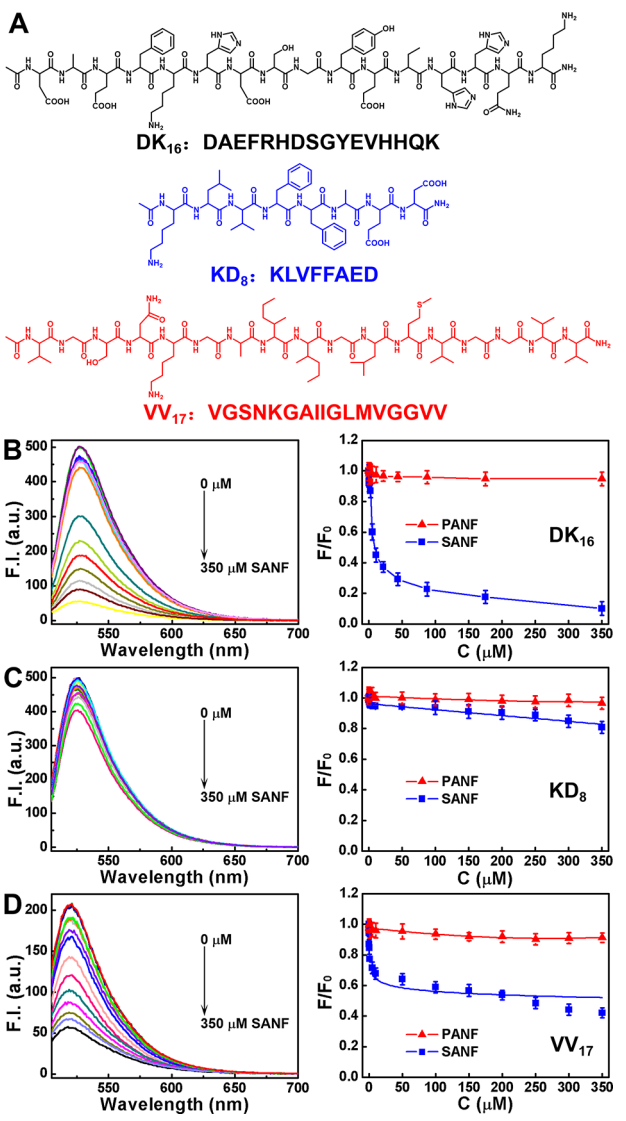

Figure 2. (A) Chemical structures of the peptides: DK$_{16}$, KD$_8$, and VV$_{17}$. (B–D) Fluorescence spectra (left) and fluorescence intensity–concentration relationship (right) of the FAM-modified (B) DK$_{16}$, (C) KD$_8$, and (D) VV$_{17}$ (7 μM) after being treated with different concentrations of SANF or PANF (0–350 μM) in 10 mM Tris-HCl buffer (pH 7.4) (λ_{ex} = 462 nm; F and F_0 represent the fluorescence intensity of FAM-modified DK$_{16}$, KD$_8$, or VV$_{17}$ with and without SANF or PANF, respectively).

rescence titration experiments were performed by preparing SANF with a series of concentrations in Tris-HCl buffer and used to investigate the fluorescence behavior of FAMDK$_{16}$, FAMKD$_8$, and FAMVV$_{17}$ in the presence of SANF. PANF without SA on the surface was used as a control. Noticeably, the fluorescence intensity of FAMKD$_{16}$ was greatly quenched along with the increase of SANF concentration as shown in Figure 2B. However, almost no FAMKD$_{16}$ fluorescence decrease in the presence of PANF was observed (Figure S21), indicating that the SA moiety of SANF was responsible for the binding due to the SA interaction with DK$_{16}$. It can be speculated that the N-terminal Aβ made a great contribution to the affinity between Aβ and SA. Next, we sought to investigate the binding ability of SA with KD$_8$. Figure 2C describes that the fluorescence of FAMKD$_8$ was slightly quenched by various concentrations of SANF or PANF, indicating that KD$_8$ may interact with SA mildly. FAMVV$_{17}$ was further used to explore the interaction between the SA on the surface of nanofiber and the C-terminal residues of Aβ peptide. Upon addition of SANF into the FAMVV$_{17}$ solution, the fluorescence signal of FAMVV$_{17}$ gradually decreased as shown in Figure 2D; however, the contrast group in the presence of PANF displayed insignificant fluorescence change (Figure S21), demonstrating the strong interaction of SANF with VV$_{17}$. From the data we can see the binding affinity followed the order of DK$_{16}$ > VV$_{17}$ > KD$_8$. The results suggest that N-terminal and C-terminal residues may contribute greatly to the high-affinity binding by hydrogen bonds and electrostatic interaction, which is consistent with the results of molecular dynamic simulations.[54,55]

Detection of Aβ_{1-40} Based on SANF and FAMVV$_{17}$. Inspired by the high binding affinity of SA with Aβ fragments of DK$_{16}$ and VV$_{17}$, we expected that the binding affinity of the full-length Aβ_{1-40} might be greatly higher than the Aβ fragments. Therefore, a competitive fluorescent turn-on method for Aβ_{1-40} detection was set up by employing the SANF-FAMVV$_{17}$ or SANF-FAMDK$_{16}$ system. Figure 3A shows that the fluorescence intensity of FAMVV$_{17}$ increases

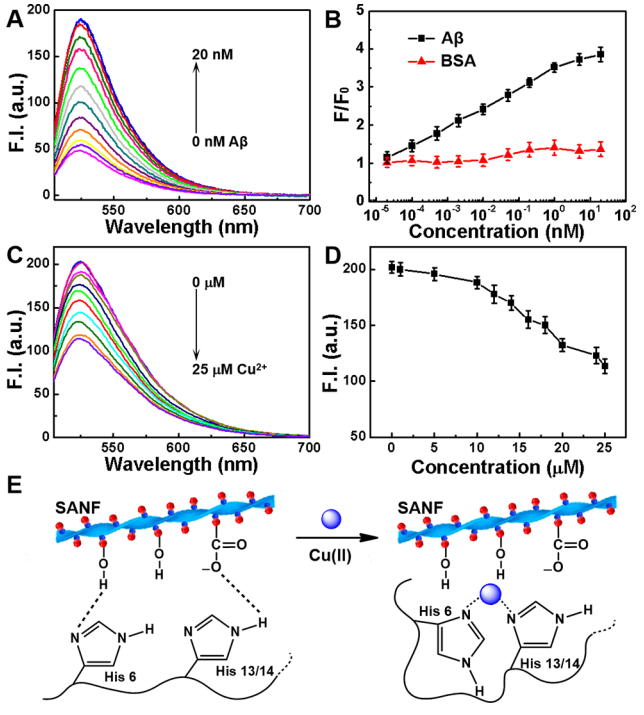

Figure 3. (A) Fluorescence spectra of FAMVV$_{17}$ (7 μM) in the presence of SANF (350 μM) and increasing concentration of Aβ monomer in 10 mM Tris-HCl buffer (pH 7.4). Aβ concentration: 0, 2 × 10^{-5}, 1 × 10^{-4}, 5 × 10^{-4}, 2 × 10^{-3}, 1 × 10^{-2}, 5 × 10^{-2}, 2 × 10^{-1}, 1, 5, and 20 nM. (B) Fluorescence intensity change vs the concentration of Aβmonomer or BSA; F and F_0 represent the fluorescence intensity of the SANF-FAMVV$_{17}$ system with and without Aβ monomers or BSA, respectively. (C) Fluorescence spectra of FAMVV$_{17}$ in the presence of SANF (350 μM), Aβ (20 nM), and increasing concentration of Cu^{2+} (0, 1, 5, 10, 12, 14, 16, 18, 20, 24, and 25 μM). (D) Fluorescence intensity change vs Cu^{2+} concentration. (E) Proposed mechanisms of Aβ/SA and Aβ/Cu^{2+} interactions.

DOI: 10.1021/acs.analchem.9b00377
Anal. Chem. XXXX, XXX, XXX–XXX

with the increase of $A\beta_{1-40}$ concentration in the range from 2×10^{-5} to 2×10^{1} nM. SANF-FAMDK$_{16}$ system responded to $A\beta_{1-40}$ in a similar way (Figure S22). The linear relationship thus spans 3 orders of magnitude before reaching a plateau at higher concentration (Figure 3B). The limit of detection was 3.8×10^{-4} nM approximately (three times the standard deviation of the blank, 3s), which is similar or superior to that reported for other assays as summarized in Table 1.

Table 1. Comparison of $A\beta_{1-40}$ Detection Performance with Other Methods

methods	detection limit	linear range	ref
LMOCP sensor	0.3 nM	1−550 nM	56
Cu^{2+} AuNP assay	0.6 nM	10.5−313.5 nM	57
STM-based immunosensor	0.23 fM	20−50 nM	58
SANF-FAMVV$_{17}$ system	3.8×10^{-4} nM	2×10^{-5}−2×10^{1} nM	this work

To evaluate the selectivity of SANF and $A\beta_{1-40}$ interaction, bovine serum albumin (BSA) comprised of 583 amino acid residues with an isoelectric point of 4.7 was tested as the possible interference. The result displayed that only a slight change in the fluorescence intensity of the SANF-FAMVV$_{17}$ system in the presence of BSA under the same conditions (Figure 3B), suggesting good selectivity for $A\beta_{1-40}$ detection. In addition, it has been well recognized that copper ions (Cu^{2+}) could bind to $A\beta$ through interaction with Asp 1, His 6, His 13, or His 14.[59] Therefore, we investigated the influence of Cu^{2+} on the fluorescence recovery ability of $A\beta_{1-40}$. As shown in Figure 3C and 3D, the fluorescence intensity decreased with the increase of the Cu^{2+} concentration compared to that without Cu^{2+}. The concentrations of Cu^{2+} added were controlled to ensure Cu^{2+} had a negligible effect on FAMVV$_{17}$ fluorescence (Figure S23). Considering that Cu^{2+} may bind to SA on the nanofiber and influence the response, control experiments of adding different concentrations of Cu^{2+} into the SANF-FAMVV$_{17}$ system in the absence of $A\beta_{1-40}$ were also performed. Cu^{2+} could induce slight fluorescence enhancement (Figure S24). Therefore, the decreased fluorescence recovery of $A\beta_{1-40}$ may be attributed to the fact that the binding of Cu^{2+} to $A\beta$ influenced the binding of $A\beta_{1-40}$ to SANF. From the results we could deduce that His 13 or His 14 was involved in the interaction between $A\beta_{1-40}$ and SA (Figure 3E).

Determination of $A\beta_{1-40}$ in Biological Samples. Encouraged by the low detection limit and high selectivity of the method, $A\beta_{1-40}$ monomer detection was also carried out in samples of artificial cerebrospinal fluid (aCSF). As illustrated in Table 2, the standard addition method analyzed by the calibration curve (Figure S25) showed acceptable recovery, which indicated the feasibility of the fluorescence analysis for $A\beta$ monomer in CSF samples using this method. Application of the method to detect $A\beta_{1-40}$ in FBS was also performed. Good recoveries were obtained and validated by ELISA assay (Table S1). The simplicity, high sensitivity, and selectivity make the fluorescence turn-on method promising as a new platform for the detection of $A\beta$ in real samples.

Table 2. Results of $A\beta_{1-40}$ Detection in aCSF

samples	added (nM)	detected (nM)	recovery (%)	RSD (%)
1	0.5	0.48 ± 0.1	95.9	3.8
2	3.0	3.1 ± 0.4	104.4	2.9
3	9.0	8.4 ± 0.6	97.1	4.7

$A\beta$ Aggregation Monitoring and Inhibitor Screening. $A\beta$ aggregation and plaque formation are implicated in AD and development of inhibitors for $A\beta$ aggregation is regarded as a potential therapy. Therefore, determination of $A\beta$ fibrillation is important for mechanism study and drug screening. For this purpose, methods with high specificity to discriminate $A\beta$ monomers and fibrils are required. Figure 4A and 4D depict

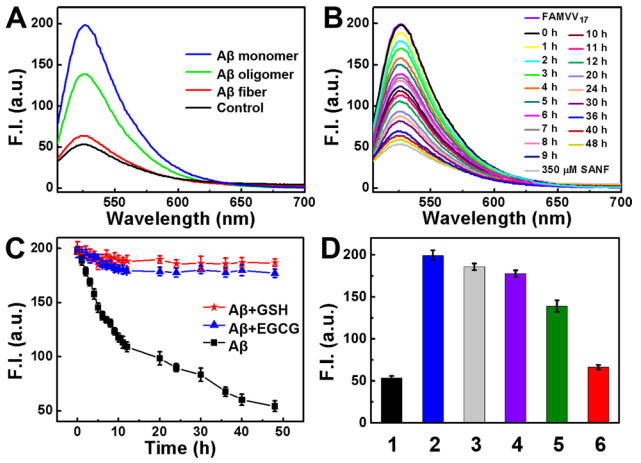

Figure 4. (A) Fluorescence spectra of FAMVV$_{17}$ (7 μM) in the presence of SANF (350 μM) upon addition of 20 nM $A\beta_{1-40}$ monomer, oligomer or fibril. (B) Fluorescence spectra of FAMVV$_{17}$ (7 μM) in the presence of SANF (350 μM) upon addition of 20 nM $A\beta_{1-40}$ incubated for different times. (C) Time-dependent fluorescence recovery of 20 nM $A\beta_{1-40}$, $A\beta_{1-40}$ in the presence of GSH, or $A\beta_{1-40}$ in the presence of EGCG. (D) Selectivity of the fluorescent turn-on assay in 10 mM Tris-HCl buffer (pH 7.4) containing 20 nM samples: (1) control, (2) $A\beta_{1-40}$ monomer, (3) $A\beta_{1-40}$ + GSH (24 h), (4) $A\beta_{1-40}$ + EGCG (24 h); (5) $A\beta_{1-40}$ oligomer (6 h); (6) $A\beta_{1-40}$ fibril (48 h).

the response of SANF-FAMVV$_{17}$ to $A\beta_{1-40}$ monomers, oligomers (incubated at 37 °C for 6 h) and fibrils (incubated at 37 °C for 48 h). The $A\beta_{1-40}$ samples incubated for 48 h showed slight fluorescence recovery compared to monomers, indicating that fibrils have less exposed interaction sites with SA. The fluorescence recovery of $A\beta_{1-40}$ sample incubated for 6 h which may contain monomers and oligomers was between that of monomers and fibrils. Then, we used the method to monitor the fibrillation of $A\beta_{1-40}$ as a function of time and the process of $A\beta_{1-40}$ aggregation was also studied by CD, thioflavin T (ThT) and atomic force microscopy (AFM) assay accordingly. As shown in Figure 4B, the silenced fluorescence signal of FAMVV$_{17}$ was rapidly recovered by $A\beta_{1-40}$ that incubated for a short time. The extent of FAMVV$_{17}$ fluorescence recovery became weaker with the prolonging of $A\beta_{1-40}$ incubation time, and after 48 h the fluorescence intensity does not show an obvious difference with the background. CD spectra showed that the typical peaks of β-sheet-rich aggregates with a maximum at 195 nm and a minimum at 215 nm increased with the increase of incubation time as well as the enhancement of ThT fluorescence (Figure S26). AFM was also used to directly visualize $A\beta$ of different morphologies by incubating $A\beta_{1-40}$ monomer in Tris-HCl for different times (Figure 5). The transitions from monomer to

DOI: 10.1021/acs.analchem.9b00377
Anal. Chem. XXXX, XXX, XXX−XXX

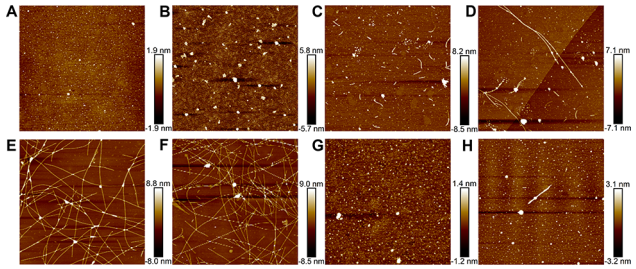

Figure 5. AFM images of Aβ samples incubated for different times in 10 mM Tris-HCl buffer (pH 7.4) with or without the presence of inhibitors: (A) 0 h, (B) 6 h, (C) 12 h, (D) 24 h, (E) 36 h, (F) 48 h, (G) Aβ_{1-40}+ EGCG 24 h, and (H) Aβ_{1-40} + GSH 24 h.

oligomer, protofibrils, and long fibrils were clearly seen. The results suggest that the fibrillation of Aβ could be monitored by this fluorescence method based on the specific interaction between Aβ and SA. Compared to the routinely used reference method, this strategy showed the advantage being sensitive, having fast response, and being suitable for high-throughput assay.

Furthermore, we continued to investigate its applicability for inhibitor screening. (−)-Epigallocatechin gallate (EGCG) and glutathione (GSH), two compounds reported to inhibit the on-pathway Aβ oligomerization and fibrillation, were chosen.[60,61] The processes of Aβ_{1-40} fibrillation in the presence of EGCG or GSH were also monitored by AFM (Figure 5G and 5H), CD, and ThT assay (Figure S26). We found that the fluorescence intensity remained high with the extension of Aβ incubation time in the presence of EGCG or GSH (Figures 4C, 4D, and S27). AFM images display that no aggregates are present in the view, implying that EGCG or GSH could exert an inhibition effect on Aβ_{1-40} aggregation. The strategy based on the specific and high-affinity binding of Aβ to SA-modified nanofiber is efficient for inhibitor screening.

CONCLUSIONS

In summary, we constructed a glycopeptide nanofiber platform by using a self-assembly method. The peptide nanofiber provided multiple SA epitopes exposed on the surface for Aβ−SA interaction analysis. By dividing Aβ_{1-40} into three fragments, we found that glycopeptide nanofiber had a high binding affinity to the N- and C-terminal domains of Aβ. We developed the system to be a fluorescent turn-on sensor to Aβ_{1-40}. It exhibited high specificity and selectivity to recognize Aβ_{1-40} monomer. It was also successfully applied to Aβ aggregation process monitoring and inhibitor screening. Further studies such as optimization of fluorophores to lower the background or developing a ratiometric response would greatly improve the analytical performace of this strategy. Therefore, this engineered carbohydrate-modified 1D nanofiber may have great potential in applications of Aβ_{1-40} detection and the early diagnosis of Alzheimer's disease.

ASSOCIATED CONTENT

Supporting Information

The Supporting Information is available free of charge on the ACS Publications website at DOI: 10.1021/acs.analchem.9b00377.

^{1}H NMR spectra of PAKL-7 and KL-7; FT-IR spectra of KL-7, PA, and PAKL-7; HRMS spectrum of KL-7 and PAKL-7; ^{1}H NMR spectra of SA-ME; ^{13}C NMR spectra of SA-ME; ^{1}H NMR spectra of Ts-SA; ^{13}C NMR spectra of Ts-SA; ^{1}H NMR spectra of N_3-SA; ^{13}C NMR spectra of N_3-SA; FT-IR spectra of SA, SA-ME, Ts-SA, and N3-SA; HRMS spectrum of SA-ME, Ts-SA, and N_3-SA; ^{1}H NMR spectra of SAKL-7; FT-IR spectra of N_3-SA, PAKL-7, and SAKL-7; HRMS spectrum of SAKL-7; zeta potential of PANF and SANF; UV−vis absorbance spectra of Neu5Ac at different concentrations in the solution containing 0.1 M $CuSO_4$, 4 % resorcinol reagent, and hydrochloric acid, corresponding calibration curve, and absorbance spectra of SANF obtained at the same condition; fluorescence spectra of $FAMDK_{16}$, $FAMKD_8$, and $FAMVV_{17}$ in the presence of different concentrations of PANF; fluorescence spectra of $FAMDK_{16}$ in the presence of SANF upon addition of Aβ monomers in 10 mM Tris-HCl buffer (pH 7.4), and fluorescence intensity change as a function of Aβ monomer concentration; fluorescence spectra of $FAMVV_{17}$ in the presence of Cu^{2+} with different concentrations in 10 mM Tris-HCl buffer (pH 7.4); fluorescence spectra and fluorescence intensity of $FAMVV_{17}$ system in the presence of SANF and Cu^{2+} with different concentrations in 10 mM Tris-HCl buffer (pH 7.4); fluorescence spectra of $FAMVV_{17}$ in the presence of SANF and Aβ_{1-40} with different concentrations in aCSF, and corresponding calibration curve; CD spectra and ThT assay of Aβ_{1-40} solutions incubated at 37 °C for different times; fluorescence spectra of $FAMVV_{17}$ in the presence of SANF upon addition of Aβ_{1-40} incubated with GSH or EGCG for different times; results of Aβ_{1-40} detection in FBS (PDF)

AUTHOR INFORMATION

Corresponding Authors

*E-mail: zaxu@chem.ecnu.edu.cn, Tel/Fax: +86-21-54340053.
*E-mail: wzhang@chem.ecnu.edu.cn, Tel/Fax: +86-21-62235761.

ORCID

Zhiai Xu: 0000-0002-4391-2507
Yang Tian: 0000-0001-8850-0349

Notes

The authors declare no competing financial interest.

ACKNOWLEDGMENTS

Financial support by the National Natural Science Foundation of China (Nos. 21675055, 21775046, 21635003) is greatly appreciated.

REFERENCES

(1) McLaurin, J.; Franklin, T.; Fraser, P.; Chakrabartty, A. *J. Biol. Chem.* **1998**, *273*, 4506−4515.
(2) Hardy, J.; Selkoe, D. J. *Science* **2002**, *297*, 353−356.
(3) Gorman, P. M.; Yip, C. M.; Fraser, P. E.; Chakrabartty, A. *J. Mol. Biol.* **2003**, *325*, 743−757.
(4) Andreasen, N.; Blennow, K. *Peptides* **2002**, *23*, 1205−1214.
(5) LaFerla, F. M.; Green, K. N.; Oddo, S. *Nat. Rev. Neurosci.* **2007**, *8*, 499−509.
(6) Benilova, I.; Karran, E.; De Strooper, B. *Nat. Neurosci.* **2012**, *15*, 349−357.
(7) Hamley, I. W. *Angew. Chem., Int. Ed.* **2007**, *46*, 8128−8147.
(8) Hardy, J.; Selkoe, D. J. *Science* **2002**, *297*, 353−356.
(9) Butterfield, S. M.; Lashuel, H. A. *Angew. Chem., Int. Ed.* **2010**, *49*, 5628−5654.

DOI: 10.1021/acs.analchem.9b00377
Anal. Chem. XXXX, XXX, XXX−XXX

(10) Härd, T. *J. Phys. Chem. Lett.* **2014**, *5*, 607−614.
(11) Zhu, L.; Zhang, J.; Wang, F.; Wang, Y.; Lu, L.; Feng, C.; Xu, Z.; Zhang, W. *Biosens. Bioelectron.* **2016**, *78*, 206−212.
(12) Zhang, J.; Liu, J.; Zhu, Y.; Xu, Z.; Xu, J.; Wang, T.; Yu, H.; Zhang, W. *Chem. Commun.* **2016**, *52*, 12044−12047.
(13) Mehta, P. D.; Pirttila, T.; Mehta, S. P.; Sersen, E. A.; Aisen, P. S.; Wisniewski, H. M. *Arch. Neurol.* **2000**, *57*, 100−105.
(14) Hardy, J.; Higgins, G. *Science* **1992**, *256*, 184−185.
(15) Zhou, Y.; Liu, L.; Hao, Y.; Xu, M. *Chem. - Asian J.* **2016**, *11*, 805−817.
(16) Yanagisawa, K.; Odaka, A.; Suzuki, N.; Ihara, Y. *Nat. Med.* **1995**, *1*, 1062−1066.
(17) Yanagisawa, K. *Glycoconjugate J.* **2015**, *32*, 87−91.
(18) Mori, K.; Mahmood, M. I.; Neya, S.; Matsuzaki, K.; Hoshino, T. *J. Phys. Chem. B* **2012**, *116*, 5111−5121.
(19) Matsuzaki, K. *Biochim. Biophys. Acta, Biomembr.* **2007**, *1768*, 1935−1942.
(20) Kreutz, F.; Frozza, R. L.; Breier, A. C.; de Oliveira, V. A.; Horn, A. P.; Pettenuzzo, L. F.; Netto, C. A.; Salbego, C. G.; Trindade, V. M. T. *Neurochem. Int.* **2011**, *59*, 648−655.
(21) Rushworth, J. V.; Hooper, N. M. *Int. J. Alzheimer's Dis.* **2011**, *2011*, 603052.
(22) Kakio, A.; Nishimoto, S. L.; Yanagisawa, K.; Kozutsumi, Y.; Matsuzaki, K. *Biochemistry* **2002**, *41*, 7385−7390.
(23) Wang, B. *Annu. Rev. Nutr.* **2009**, *29*, 177−222.
(24) Ariga, T.; Yu, R. K. *Neurochem. Res.* **1999**, *24*, 219−226.
(25) Wakabayashi, M.; Okada, T.; Kozutsumi, Y.; Matsuzaki, K. *Biochem. Biophys. Res. Commun.* **2005**, *328*, 1019−1023.
(26) Schladitz, C.; Vieira, E.; Hermel, H.; Mohwald, H. *Biophys. J.* **1999**, *77*, 3305−3310.
(27) Williams, T. L.; Serpell, L. C. *FEBS J.* **2011**, *278*, 3905−3917.
(28) Matsuzaki, K.; Noguch, T.; Wakabayashi, M.; Ikeda, K.; Okada, T.; Ohashi, Y.; Hoshino, M.; Naiki, H. *Biochim. Biophys. Acta, Biomembr.* **2007**, *1768*, 122−130.
(29) Amaro, M.; Sachl, R.; Aydogan, G.; Mikhalyov, I. I.; Vácha, R.; Hof, M. *Angew. Chem., Int. Ed.* **2016**, *55*, 9411−9415.
(30) Matsubara, T.; Nishihara, M.; Yasumori, H.; Nakai, M.; Yanagisawa, K.; Sato, T. *Langmuir* **2017**, *33*, 13874−13881.
(31) Vahed, M.; Neya, S.; Matsuzaki, K.; Hoshino, T. *J. Phys. Chem. B* **2018**, *122*, 3771−3781.
(32) Williamson, M. P.; Suzuki, Y. U.; Bourne, N. T.; Asakura, T. *Biochem. J.* **2006**, *397*, 483−490.
(33) Kelm, S.; Schauer, R. *Int. Rev. Cytol.* **1997**, *175*, 137−240.
(34) Crocker, P. R.; Paulson, J. C.; Varki, A. *Nat. Rev. Immunol.* **2007**, *7*, 255−266.
(35) Wittmann, V.; Pieters, R. J. *Chem. Soc. Rev.* **2013**, *42*, 4492−4503.
(36) Gestwicki, J. E.; Cairo, C. W.; Strong, L. E.; Oetjen, K. A.; Kiessling, L. L. *J. Am. Chem. Soc.* **2002**, *124*, 14922−14933.
(37) Battigelli, A.; Kim, J. H.; Dehigaspitiya, D. C.; Proulx, C.; Robertson, E. J.; Murray, D. J.; Rad, B.; Kirshenbaum, K.; Zuckermann, R. N. *ACS Nano* **2018**, *12*, 2455−2465.
(38) Lee, S. S.; Fyrner, T.; Chen, F.; Álvarez, Z.; Sleep, E.; Chun, D. S.; Weiner, J. A.; Cook, R. W.; Freshman, R. D.; Schallmo, M. S.; Katchko, K. M.; Schneider, A. D.; Smith, J. T.; Yun, C.; Singh, G.; Hashmi, S. Z.; McClendon, M. T.; Yu, Z.; Stock, S. R.; Hsu, W. K.; Hsu, E. L.; Stupp, S. I. *Nat. Nanotechnol.* **2017**, *12*, 821.
(39) Muñoz, A.; Sigwalt, D.; Illescas, B. M.; Luczkowiak, J.; Rodríguez-Pérez, L.; Nierengarten, I.; Holler, M.; Remy, J. S.; Buffet, K.; Vincent, S. P.; Rojo, J.; Delgado, R.; Nierengarten, J. F.; Martín, N. *Nat. Chem.* **2016**, *8*, 50−57.
(40) Dai, B.; Li, D.; Xi, W.; Luo, F.; Zhang, X.; Zou, M.; Cao, M.; Hu, J.; Wang, W.; Wei, G.; Zhang, Y.; Liu, C. *Proc. Natl. Acad. Sci. U. S. A.* **2015**, *112*, 2996−3001.
(41) Lock, L. L.; Reyes, C. D.; Zhang, P.; Cui, H. *J. Am. Chem. Soc.* **2016**, *138*, 3533−3540.
(42) Sun, H. L.; Chen, Y.; Han, X.; Liu, Y. *Angew. Chem.* **2017**, *129*, 7168−7171.
(43) Qi, G. B.; Gao, Y. J.; Wang, L.; Wang, H. *Adv. Mater.* **2018**, *30*, 1703444.
(44) Svennerholm, L. *Biochim. Biophys. Acta* **1957**, *24*, 604−611.
(45) Safaryan, S.; Slabov, V.; Kopyl, S.; Romanyuk, K.; Bdikin, I.; Vasilev, S.; Zelenovskiy, P.; Shur, V. Y.; Uslamin, E. A.; Pidko, E. A.; Vinogradov, A. V.; Kholkin, A. L. *ACS Appl. Mater. Interfaces* **2018**, *10*, 10543−10551.
(46) Lee, J. H.; Heo, K.; Schulz-Schönhagen, K.; Lee, J. H.; Desai, M. S.; Jin, H. E.; Lee, S. W. *ACS Nano* **2018**, *12*, 8138−8144.
(47) Almohammed, S.; Oladapo, S. O.; Ryan, K.; Kholkin, A. L.; Rice, J. H.; Rodriguez, B. J. *RSC Adv.* **2016**, *6*, 41809−41815.
(48) Rengifo, R. F.; Li, N. X.; Sementilli, A.; Lynn, D. G. *Org. Biomol. Chem.* **2017**, *15*, 7063−7071.
(49) Kapil, N.; Singh, A.; Das, D. *Angew. Chem.* **2015**, *127*, 6592−6595.
(50) Omosun, T. O.; Hsieh, M. C.; Childers, W. S.; Das, D.; Mehta, A. K.; Anthony, N. R.; Pan, T.; Grover, M. A.; Berland, K. M.; Lynn, D. G. *Nat. Chem.* **2017**, *9*, 805−809.
(51) Miyazawa, T. *J. Chem. Phys.* **1960**, *32*, 1647−1652.
(52) Mehta, A. K.; Lu, K.; Childers, W. S.; Liang, Y.; Dublin, S. N.; Dong, J.; Snyder, J. P.; Pingali, S. V.; Thiyagarajan, P.; Lynn, D. G. *J. Am. Chem. Soc.* **2008**, *130*, 9829−9835.
(53) Lu, K.; Jacob, J.; Thiyagarajan, P.; Conticello, V. P.; Lynn, D. G. *J. Am. Chem. Soc.* **2003**, *125*, 6391−6393.
(54) Vahed, M.; Neya, S.; Matsuzaki, K.; Hoshino, T. *J. Phys. Chem. B* **2018**, *122*, 3771−3781.
(55) Hoshino, T.; Mahmood, M. I.; Mori, K.; Matsuzaki, K. *J. Phys. Chem. B* **2013**, *117*, 8085−8094.
(56) Liu, B.; Shen, H.; Hao, Y.; Zhu, X.; Li, S.; Huang, Y.; Qu, P.; Xu, M. *Anal. Chem.* **2018**, *90*, 12449−12455.
(57) Zhou, Y. L.; Dong, H.; Liu, L. T.; Xu, M. T. *Small* **2015**, *11*, 2144−2149.
(58) Prabhulkar, S.; Piatyszek, R.; Cirrito, J. R.; Wu, Z. Z.; Li, C. Z. *J. Neurochem.* **2012**, *122*, 374−381.
(59) Faller, P.; Hureau, C.; La Penna, G. *Acc. Chem. Res.* **2014**, *47*, 2252−2259.
(60) Ehrnhoefer, D. E.; Bieschke, J.; Boeddrich, A.; Herbst, M.; Masino, L.; Lurz, R.; Engemann, S.; Pastore, A.; Wanker, E. E. *Nat. Struct. Mol. Biol.* **2008**, *15*, 558−566.
(61) More, S. S.; Vartak, A. P.; Vince, R. *ACS Chem. Neurosci.* **2013**, *4*, 330−338.

DOI: 10.1021/acs.analchem.9b00377
Anal. Chem. XXXX, XXX, XXX−XXX